www.sciencemag.org/content/353/6299/579/suppl/DC1

Supplementary Materials for

Outburst flood at 1920 BCE supports historicity of China's Great Flood and the Xia dynasty

Qinglong Wu,* Zhijun Zhao, Li Liu, Darryl E. Granger, Hui Wang, David J. Cohen, Xiaohong Wu, Maolin Ye, Ofer Bar-Yosef, Bin Lu, Jin Zhang, Peizhen Zhang, Daoyang Yuan, Wuyun Qi, Linhai Cai, Shibiao Bai

*Corresponding author. Email: wuqinglong@pku.edu.cn

Published 5 August 2016, *Science* **353**, 579 (2016)
DOI: 10.1126/science.aaf0842

This PDF file includes:

Materials and Methods
Figs. S1 to S7
Tables S1 to S5
References

Materials and Methods

1. Reconstruction of the Jishi Gorge landslide dam geometry

The remnant dam was identified by field investigation and inspection with Google Earth (Fig. S2A). The upstream limit of the dam (part A) reaches 85 m arl on the right bank, slopes steeply upstream, and is covered by lacustrine sediments; it was previously identified (*17*) as a landslide dam without recognizing that it was part of a larger body. The main remnant dam (part B) is found on the left bank, reaches 240 m arl and stretches for over a kilometer of river distance. Both dam remnants are composed of landslide debris and shattered bedrock. The source of the landslide must have been the right bank, where a landslide scar forms the ridge crest. No such scars are found elsewhere around the remnant dam (Fig. S2A, B). The original dam would have been 700-800 m across and ca. 1,300 m long (Fig. S2A). Reconstruction of the former surface indicates a surface slope of 0.28-0.32, near the angle of repose. Based on the dam geometry and the valley topography, the volume of the dam is roughly estimated to be 4-8 × 10^7 m^3 (Table S1).

The depth of the lake impounded by the dam depends on the minimum height of the dam at its saddle. The saddle's surface must have been lower than the preserved remnants of the dam. Because the crest of the dam remnants is very gentle, we interpolate a surface with a saddle ca. 30-55 m lower than the preserved surface, making the lake elevation 2,000-2,025 m asl (185-210 m arl) (Fig. 1B, S2B).

2. Reconstruction of the dammed lake, breach depth, and the outburst volume

Using the reconstructed dam elevation of 2,000-2,025 m asl, we used topographic data from the Shuttle Radar Topography Mission (SRTM) (*33*) and ArcGIS software to reconstruct the extent and volume of water impounded. At the time of overtopping the lake volume would have been 12.0-16.8 km^3. Widespread lacustrine sediments upstream of the dam reach an elevation of 1890 m asl (Fig.S3A, B), indicating that a lower part of the dam remained for many years after the catastrophic breaching event. The volume of this lower lake would have been 0.7 km^3. From the difference in lake volumes we infer that the dam breach would have released from 11.3-16.1 km^3 of water in the outburst flood (Table S1).

The time required to infill the lake can be estimated from the average discharge of the Yellow River at the dam site. The modern average annual discharge is ca. 730 m^3s^{-1}, indicating that it would take from 6-9 months to fill the lake.

3. Estimation of the maximum discharge of the breach flow at the dam

Reconstructing the discharge of catastrophic dam failures is subject to considerable uncertainty. We employ two independent approaches. The first is based on the dam and lake geometries, and the second is based on reconstructions of the outburst flood channel downstream.

There are many empirical regressions to estimate outburst flood discharge from parameters such as outburst volume (V), dam height (h), depth of the breach (d), and potential energy of the impounded waters (PE). Regressions using one parameter tend to have 95% confidence intervals ranging over approximately an order of magnitude and may underestimate large floods, while multiple regressions tend to do better, with typical

uncertainties within a factor of 2-5 (*34, 35*). Recognizing these very high uncertainties, we calculate peak discharge using a variety of empirical regressions (Table S3) (*36-38*). Peak discharges from the regressions range from 0.08-0.38×10^6 m^3s^{-1} for the lower dam height condition and 0.12-0.51×10^6 m^3s^{-1} for the higher condition. In general, outburst floods tend to be larger for failures that occur with a high ratio of lake volume to dam volume. For the Jishi flood the outburst volume is approximately 140-200 times larger than the dam volume, so we might expect the discharge to lie within the higher range of the empirical estimations.

The maximum permissible discharge for the dam break can be estimated using the Ritter (1892) approximation (*39*), which assumes critical flow through a rectangular frictionless and instantaneous dam breach. For the lower condition, we obtain a maximum discharge of 0.26×10^6 m^3s^{-1} assuming a breach that is 330 m wide and 90 m deep (20 m less than the final breach depth of 110 m). For the upper condition, we obtain a maximum discharge of 0.46 × 10^6 m^3s^{-1} assuming a breach width of 405 m and a depth of 115 m (20 m less than the final breach depth).

4. Estimation of the peak discharge of the outburst flood with Manning's equation

A more reliable way to estimate paleo-discharge of the flood is by using Manning's equation to estimate flow velocity at a reconstructed cross section. The peak discharge of the flood is then estimated with Q=Av, where Q is the discharge (m^3s^{-1}), A is the area (m^2) of cross section of flow, and v is mean flow velocity (ms^{-1}). By substituting v from Manning's equation (*40*), discharge is expressed as $Q=n^{-1}R^{2/3}S^{1/2}A$. In this formula, n is Manning's roughness coefficient, S is the energy slope, and R is the hydraulic radius (m), given by R=A/L, where L is the wetted perimeter of the cross section. We reconstructed a cross section of the flood where it passed the Lajia site in the Guanting Basin.

Outburst flood sediment has been preserved at the Lajia site and at the cross section line AB (Fig. 1A). The OFS was buried by mudflow deposits and has been re-exposed by gully erosion and archaeological excavations (Fig. S6A, B). We reconstructed the channel cross section by surveying the base of the OFS using a Differential Global Positioning System (Fig. S6C). The height of the flood is best represented by the highest occurrence of OFS. On the north side of the river, near point A of the cross section (Fig. S6), the OFS fills a ground fissure and reaches an elevation of 1799.5 m asl. On the south end of the cross section, near point B a thin OFS sheet reaches 1799.6 m asl. At a third site, 30 m south of point A, an OFS lens with thickness of ca. 0.5 m revealed by archaeological excavation (Fig. S6A) reaches ca. 1798.0 m asl. Since the highest elevation of the OFS might not have been revealed or observed, the level of the outburst flood at peak stage may safely be taken as 1800 m asl.

We also must consider the widening and incision of the valley after the outburst flood of the Yellow River. We assume that the bottom of the outburst flood at the cross section at peak stage was 1770 m asl, 8 m above the present water level (1762 m asl), based on observations at a location about 2 km upstream (P11 in Fig. 1A), where the elevation of the OFS is 7 m above the present Yellow River. As lateral erosion in the Guanting Basin by the Yellow River has occurred in modern times, we assume that the terrace occupied by the Lajia site has been eroded laterally by a width of 140 meters (i.e.

the width of the Yellow River channel) after the outburst flood. Our reconstructed cross section of the outburst flood at peak stage has a total area of 47,100 m^2 at the Lajia site (Fig. S6C).

We compute the peak discharges of the outburst flood at this cross section using values of Manning's n varying from 0.02-0.05 (Table S4). The highest calculated discharge is 0.72×10^6 m^3s^{-1} for n=0.02, while the lowest is 0.29×10^6 m^3 s^{-1} for n=0.05. Considering that observed roughness coefficient n during modern floods in the upper Yellow River ranges from 0.019 to 0.041 (*41*), n=0.03-0.04 is reasonable for the outburst flood, and thus the peak discharge ranges between 0.36×10^6 to 0.48×10^6 m^3s^{-1}. The best estimate of peak discharge using Manning's equation is thus near 0.4×10^6 m^3s^{-1}, consistent with the empirical estimations from dam failure.

5. Radiocarbon dating

The flood was dated using radiocarbon dating of charcoal and bone. During sampling of charcoal from sediment, all the strata were examined carefully to make sure that the charcoal fragments and other materials for radiocarbon dating were not intrusive bodies.

Sample pretreatment was performed in the Archaeological Lab, School of Archaeological and Museum Studies, Peking University. The charcoal samples were pretreated using the acid-alkali-acid (AAA) sequence to remove contaminants (*42*). Surfaces of the three bone samples were cleaned and broken into small pieces and then were treated with AAA procedures to extract the bone collagen (*43*). The gelatin from the bone samples was obtained through centrifugation and lyophilized. The ratios of carbon to nitrogen (C/N value) for the gelatin samples were measured and evaluated (only the samples with C/N within 2.9-3.6 were selected for AMS ^{14}C measurement) (*44*). These selected samples were transformed into graphite following standard procedures (*45*, *46*). The AMS radiocarbon measurements of the prepared graphite samples were performed at the AMS Center, School of Physics, Peking University (BA). The AMS system is based on a National Electrostatics Corp. (NEC) 1.5SDH-1 0.5MV pelletron with 40-sample MC-SNICS ion source. The accuracy of this system is better than 0.4% and the machine background is lower than 0.03pMC. The ^{14}C ages of the samples were determined with Libby half-life (5,568 years), the Northern Hemisphere ^{14}C calibration curve Intcal13 (*31*) and OxCal v 4.2 (*32*).

Provided there are no postdepositional formation processes working on flood sediments, such as bioturbation, the calibrated radiocarbon ages of charcoal fragments found within the sediments will be older than the formation of the deposits in which they are found. That is to say, the flood cannot be older than the most recent charcoal found within its sediments, provided the flood contexts are undisturbed (and so the charcoal samples provide a *terminus post quem*). For a cataclysmic flood, radiocarbon dates might be much older than the flood itself, as the forces of the flood can rework much older deposits and redeposit charcoal fragments from them. Of course, if the sample number is small, even the most recent calibrated age may be much older than the true age of the outburst flood. Sample L-11, with a calibrated 2σ age interval from 2129-1892 BC provides the best *terminus post quem* from the OFS. A single sample from a silty layer above the OFS (L-16) has a slightly younger calibrated age range of 2010-1770 BC

consistent with the date of the flood inferred from L-11, but it does not provide a tight age control (*terminus ante quem*) because the charcoal could be reworked.

The best age for the flood comes from dating the collapse of the dwellings at Lajia, which occurred within a year prior to the flood, and the same earthquake that collapsed the cave dwellings likely triggered the landslide dam. Bone samples from three children (6-13 years old) (Fig. 2B) killed by the collapse of the cave dwellings during the earthquake (*18, 30*) were dated and yield indistinguishable radiocarbon ages, Because the three children died at the same time and because their bones reflect recent growth, their $^{14}C/^{12}C$ ratio should be practically identical and can be considered replicates. We calculated an inverse variance weighted mean for the three samples of 3573 ± 18 ^{14}C yrs. This corresponds to a calibrated age range (95.2%) of 1882-1976 BC. The samples fall within a linear portion of the calibration curve, yielding a symmetric calibrated age distribution, with a median age of 1922 ± 28 BC (1σ).

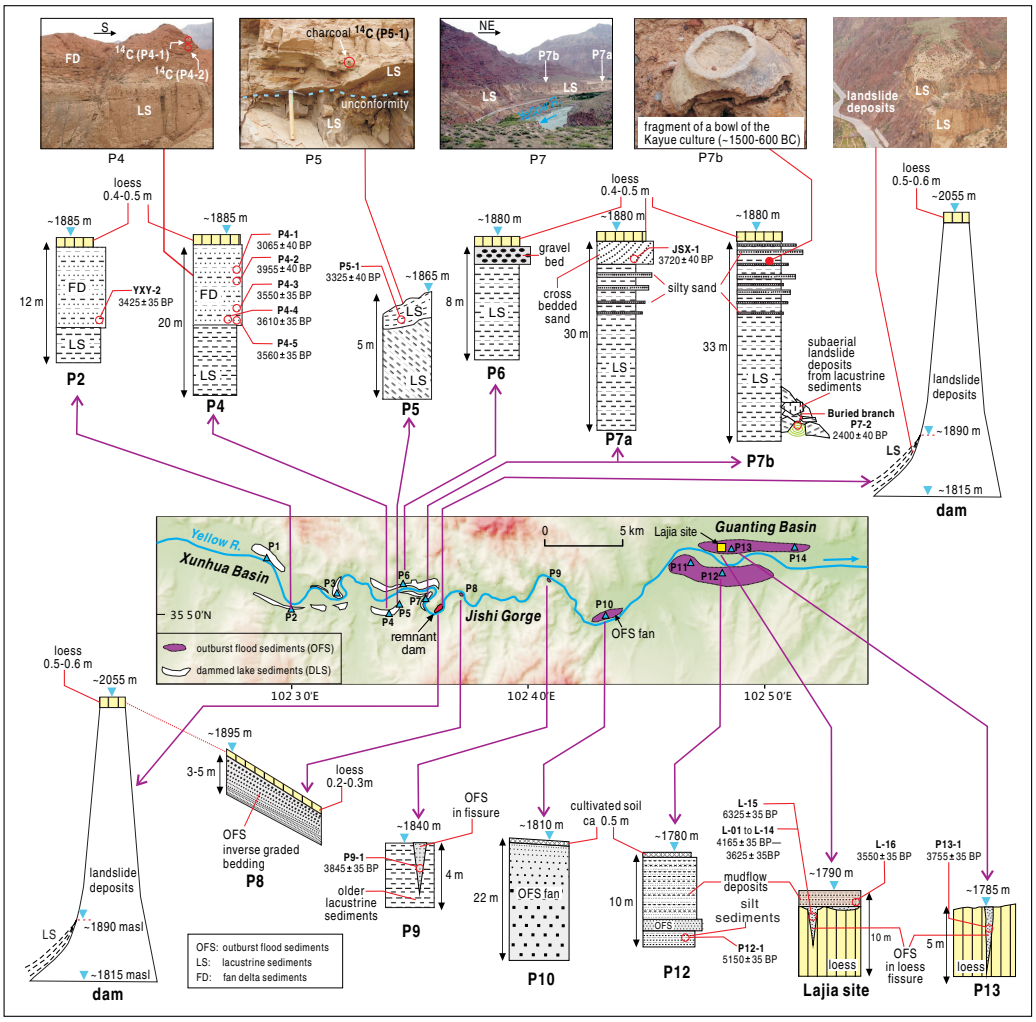

Fig. S1.

Stratigraphic relations of DLS, remnant dam and OFS. The map indicates the distribution of the dammed lake sediments (DLS), remnant dam and outburst flood sediments (OFS) in the Jishi Gorge and vicinity. Above the map are stratigraphic sections of DLS and their relation to the dam. Below the map are stratigraphic sections of OFS and their relation to the dam. The small red circles show the locations of the charcoal samples. Two charcoal ages (in profile P2 and P7a) are from a previous study (*17*). The unconformity in profile P5 probably resulted from a subaqueous slump as no pedogenic characteristics or loess has been observed and no fault has been found. The loess accumulation rate in the Holocene in the upper region of the Yellow River is ~0.1-0.2 m/ka, showing that the formation of the dam, the occurrence of the outburst flood and the disappearance of the lake were later than 0.5 ka BP. The loess on OFS at P8 is only 0.2-0.3 m, because loess on a sloping surface is vulnerable to erosion. The pottery bowl fragment buried in the top part of the DLS (P7b) shows that the final disappearance of the residual lake should be within the range of ~1500-600 BC (~3450-2550 BP), based on the dating of the archaeological Kayue culture from which the pottery bowl derives.

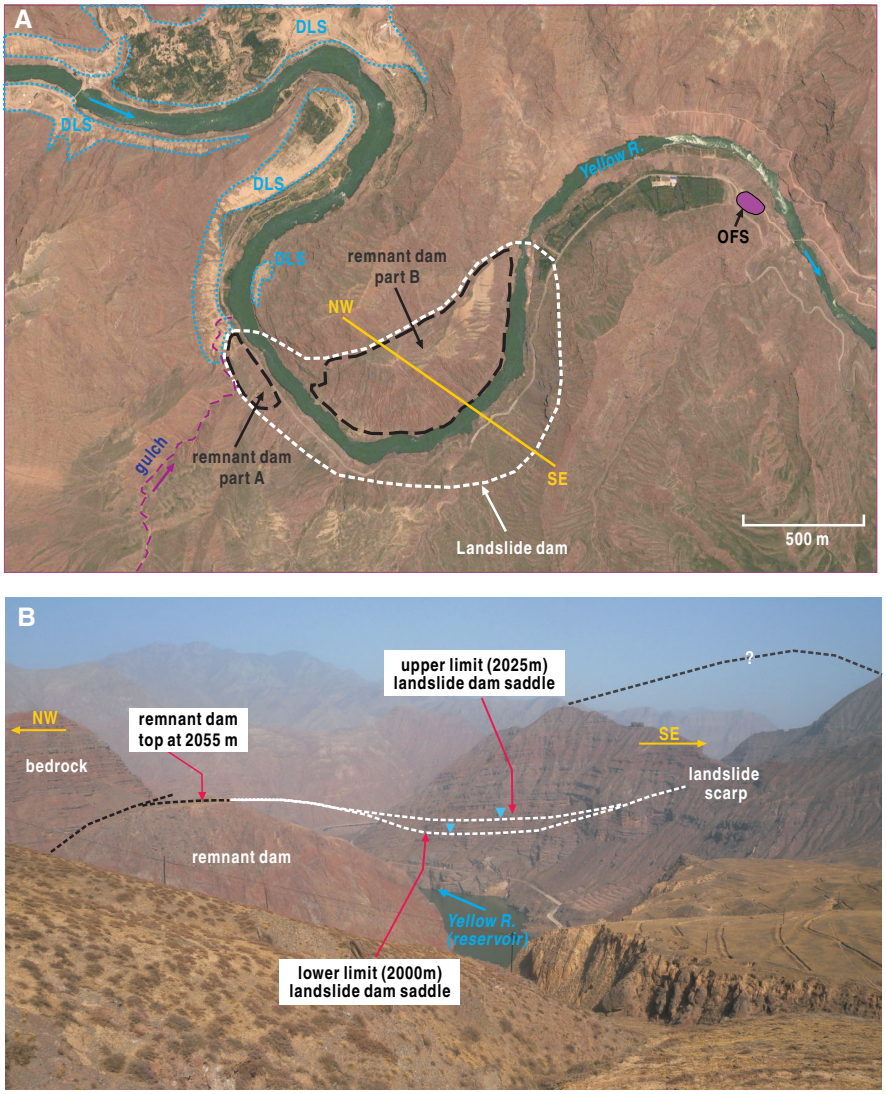

Fig. S2

The prehistoric landslide dam in the Jishi Gorge. (**A**) Image from Google Earth showing the location of the remnant dam (black dashed line) in the Jishi Gorge, and extent of the reconstructed landslide dam (white dotted line). (**B**) Photo looking downstream showing the topography near the remnant dam. The white dotted lines indicate the reconstructed lower and upper conditions of the saddle of the landslide dam.

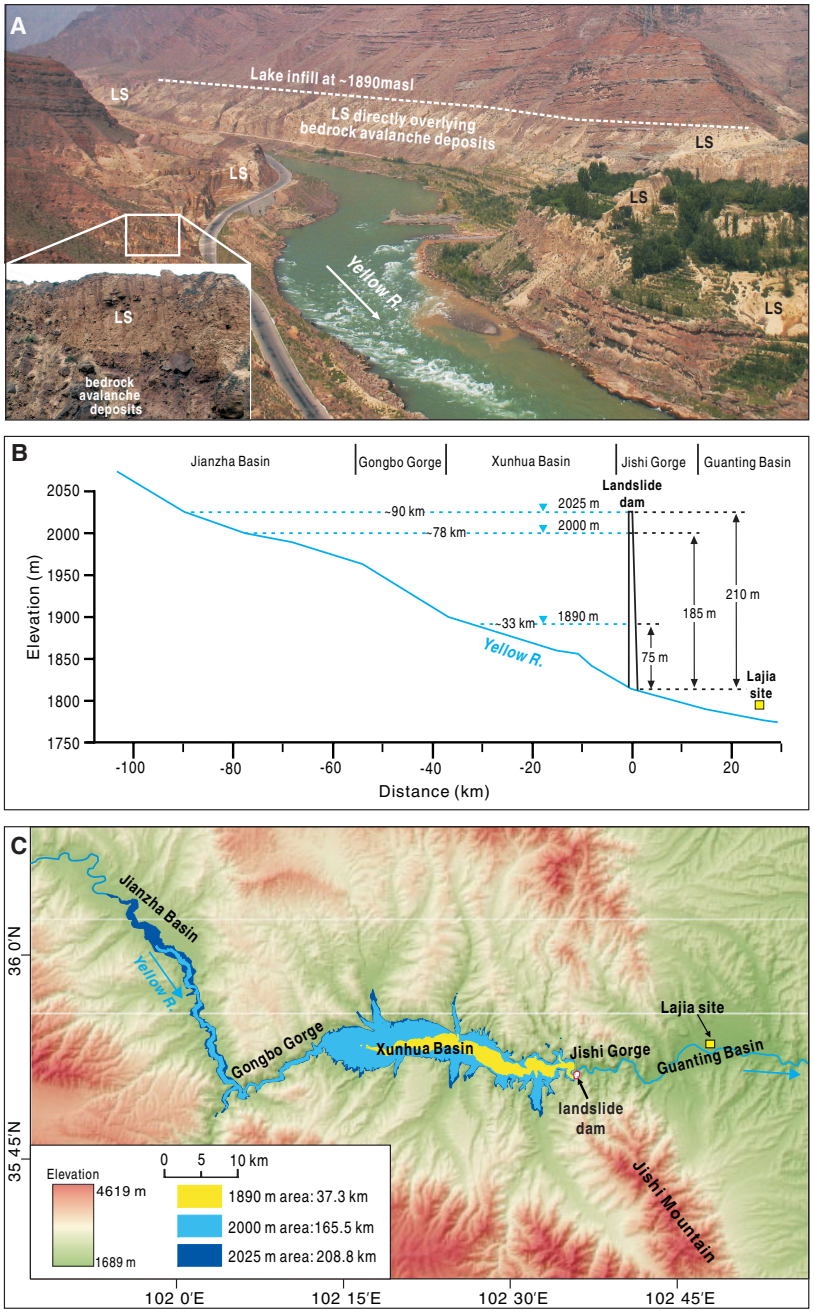

Fig. S3

Reconstruction of the landslide dammed lake. (A) Photo in west Jishi Gorge showing the infilling of lacustrine sediment up to 1,890 m asl as a geomorphic marker to indicate the remnant dam elevation after breach (LS = Lacustrine Sediment). **(B)** The extent of the dammed lake relative to the longitudinal profile of the Yellow River. The lower (2,000 m asl, 185 m arl) and upper (2,025 m asl, 210 m arl) scenarios are shown. **(C)** The extent of the residual lake after the outburst flood is shaded in yellow, at an elevation of 1,890 m asl.

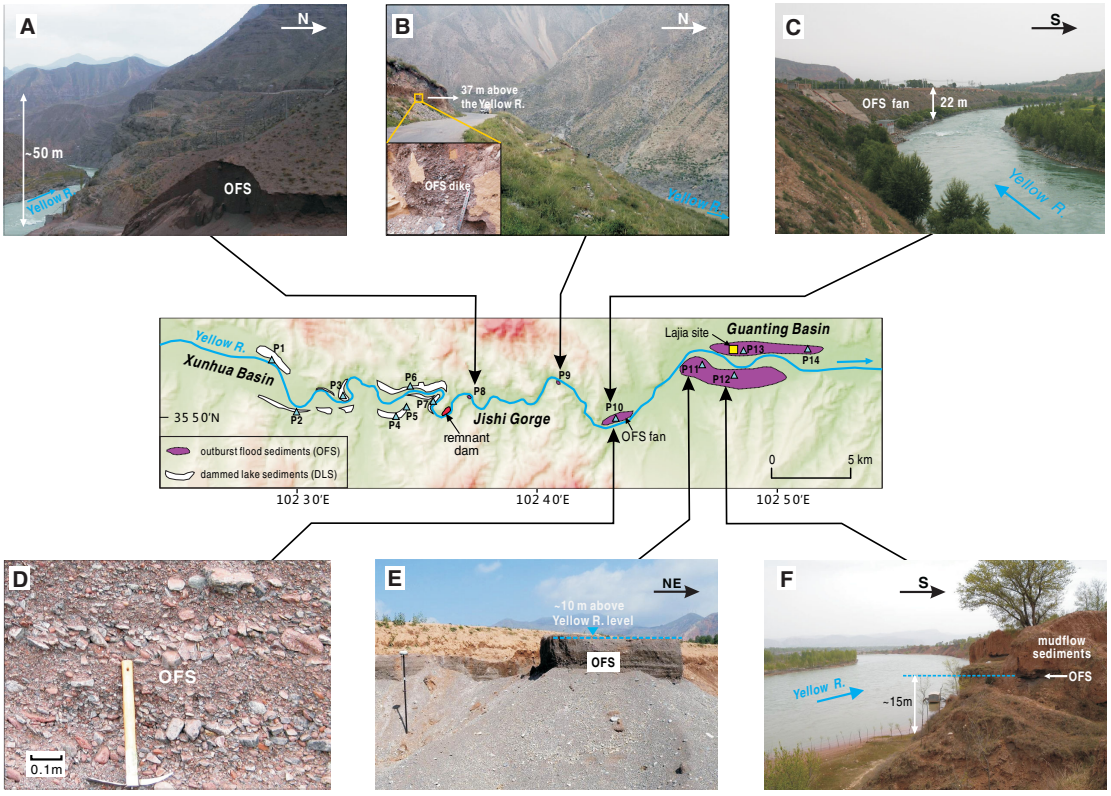

Fig. S4

OFS in Jishi Gorge and Guanting Basin. (**A**) OFS at ~50 m arl in Jishi Gorge, ~1.2 km downstream from the landslide dam. It is characterized by coarsening upward, well-sorted angular sandy to fine gravel clasts of purple-brown mudrocks with bedding parallel to the hill slope. No greenschist is included here because it outcrops further downstream (see fig.1A). The OFS is covered by ~0.2-0.3 m thick loess. The view is downstream. (**B**) Sandy-gravel OFS at 37 m arl overlapping and filling in a fissure in older lacustrine sediments in Jishi Gorge, ~8 km downstream of the dam. The OFS is composed of angular greenschist and mudrock clasts with diameters of up to 50 mm. (**C**) OFS fan located at the outlet of Jishi Gorge. The deposit is up to ~20 m thick, and its surface is ~22 m arl. It is characterized by horizontally bedded silt to boulders with diameter up to 2 m, typical of condensed suspension deposit. (**D**) Close-up of an outcrop of the OFS fan. The gravel-pebble-cobble sediments consist almost entirely of clasts of greenschist and purple-brown mud-rock. Outsized boulders with diameters larger than 1 m appear commonly in the matrix. (**E**) Pure sandy-gravel OFS sheet of horizontal stratification in the Guanting Basin. View direction is northwest (upstream). (**F**) Pure sandy-gravel OFS sheet 15 m arl covered by mudflow sediments with thickness of up to 3-5 m.

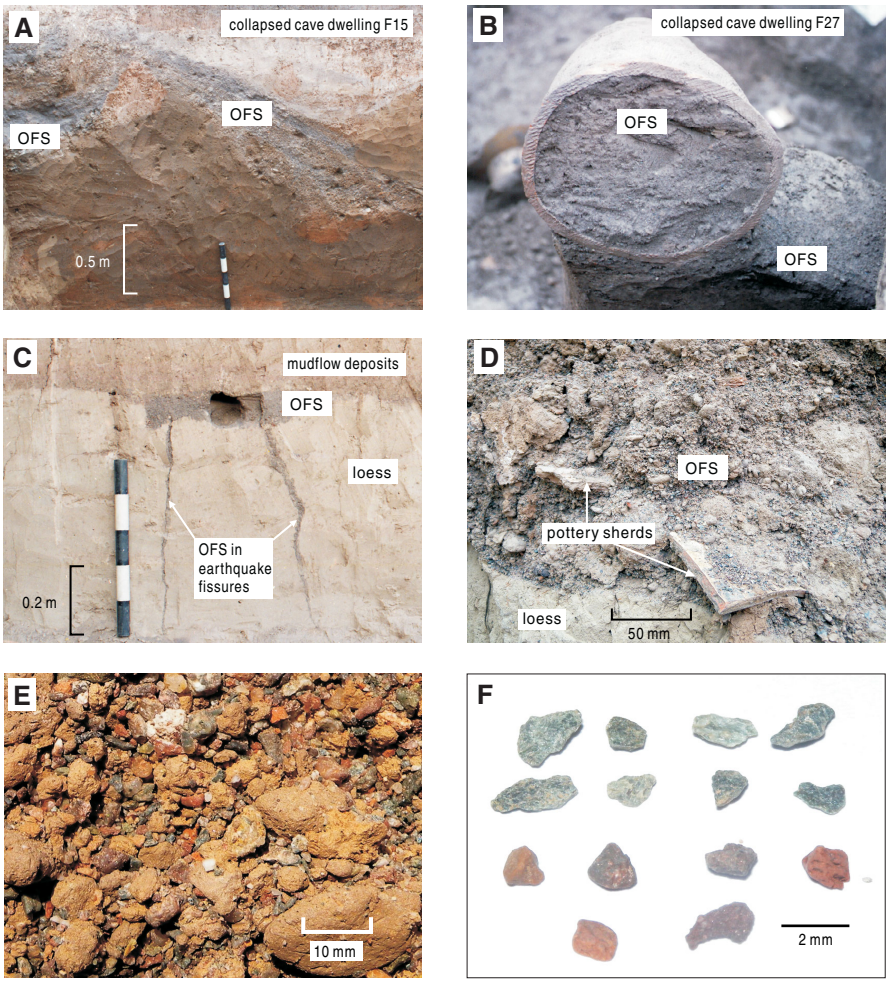

Fig. S5

Features of OFS at the Lajia site. (**A**) Sandy OFS in the collapsed cave dwelling labeled F15. (**B**) OFS underlying and filling a well preserved pottery jar in a cave dwelling. (**C**) Earthquake fissures in loess filled in with sandy OFS dikes and covered by mudflow. (**D**) OFS mixed with pottery sherds and other cultural material clasts overlying loess. (**E**) Close view of OFS composed of greenschist, mudrock clasts and rounded mud balls reworked from underlying loess. **(F)** Angular clasts of greenschist clasts (upper two rows) and mudrock clasts (lower two rows).

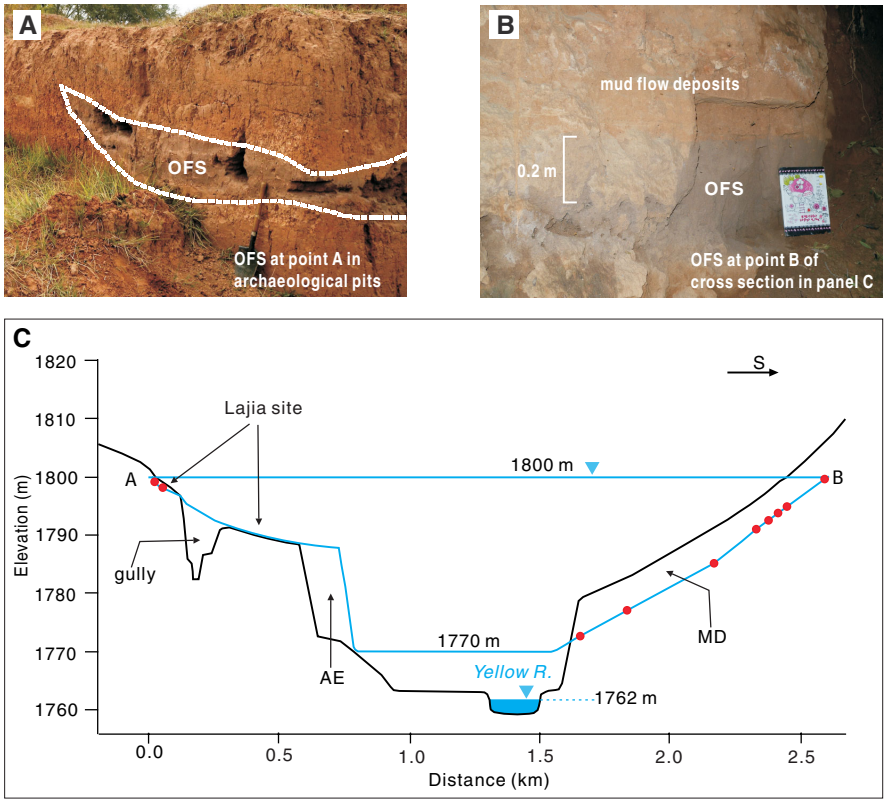

Fig. S6

Cross section reconstruction of the outburst flood at peak stage in Guanting Basin. (**A**) OFS lens revealed by archaeological excavation at elevation of ~1,798 m asl near the Lajia site on the left bank of the Yellow River. **(B)** OFS sheet outcropped by gulch incision at ~1,799 m asl on the right bank of the Yellow River. **(C)** Reconstructed cross section of the outburst flood at peak stage 25 km downstream of the dam. Red dots represent the position of OFS bottom measured using differential GPS. The blue line shows the outline of the reconstructed cross section, with 1,800 m asl as the flood surface and 1,770 m asl as bottom. Black line shows the modern topographic section. The area enclosed by the blue and black lines denoted by AE represents part of the terrace eroded after the outburst flood. MD: mudflow deposits overlying OFS.

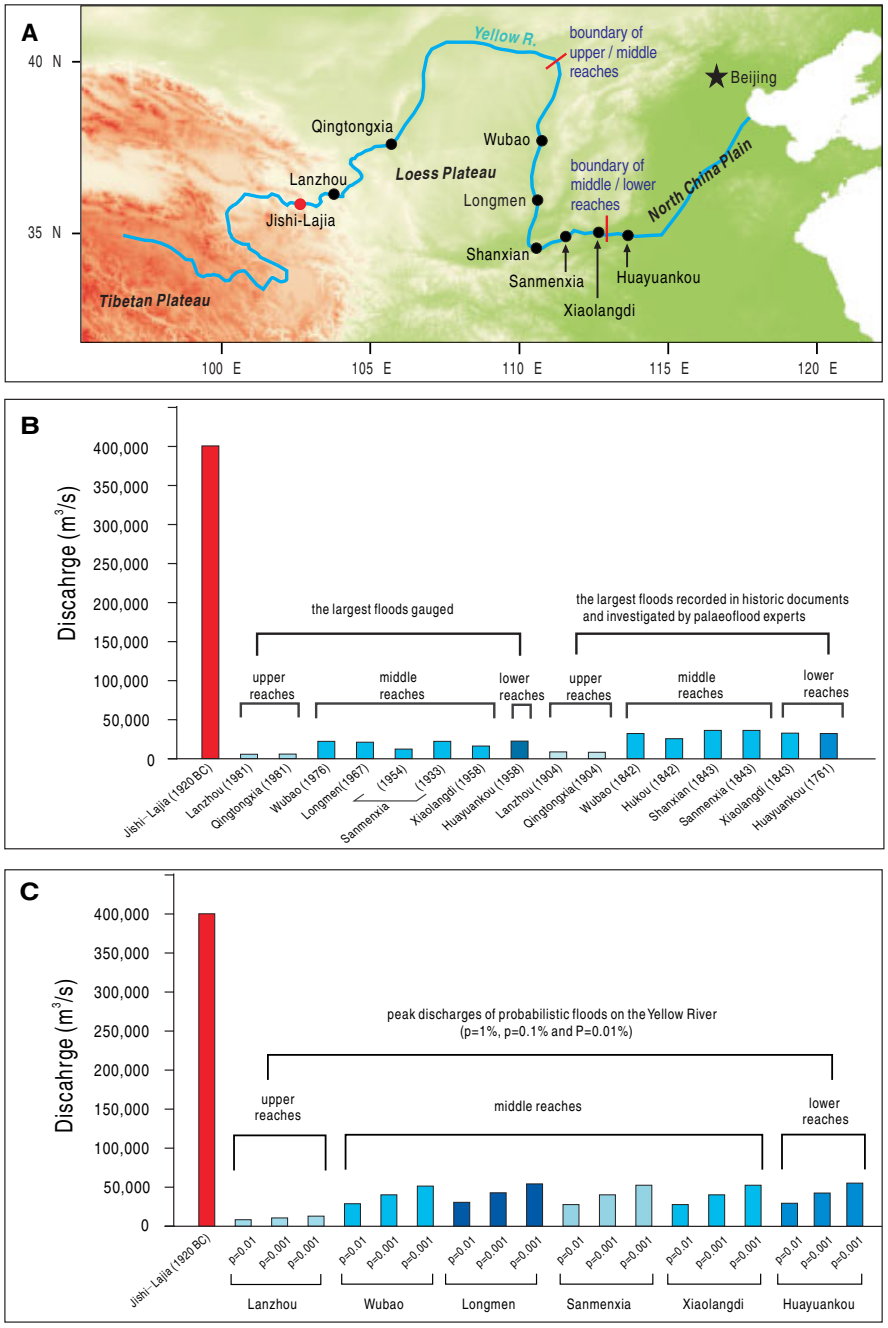

Fig. S7

Comparison of the prehistoric Jishi-Lajia outburst flood with the largest historical floods (A) and the probabilistic floods (B) on the Yellow River. Here 0.4×10^6 m^3s^{-1} is taken as the peak discharge of the outburst flood. The data of the largest historical floods (LHFs) are from (*41*) and probabilistic floods are from (*47*).

Table S1.

Parameters of the landslide dam reconstructions used to estimate breach discharge.

Parameters of the dammed lake	Value of parameters	
Remnant dam surface elevation	2,055 m asl	
Dam length (along the valley)	~1,300 m	
Dam width (across the valley)	700-800 m	
Volume of the landslide dam	$V_d=4\times10^7$-8×10^7 m^3	
	Lower condition	Upper condition
Saddle elevation (maximum lake level)	H=2,000 m asl	H=2,025 m asl
Dam height (bottom to saddle)	h=185 m	h=210 m
Maximum surface area of dammed lake	A_s=166 km^2	A_s=209 km^2
Maximum volume impounded	$V_m=1.20\times10^{10}$ m^3	$V_m=1.68\times10^{10}$ m^3
Outburst volume	$V_o=1.13\times10^{10}$ m^3	$V_o=1.61\times10^{10}$ m^3
Breach depth	d=110 m	d=135 m
Gradient of the downslope of dam	s=0.28	s=0.32
Ratio of outburst volume to dam volume	141-282	200-400

Table S2.

The lithologic composition OFS samples from Lajia site and Guanting Basin.

Sample No.	sampling location	sample number (n)	clast diameter (mm)	greenschist clasts content (%)	purple-brown mudrock clasts content (%)	other types of clasts content (%)
SS1	Lajia site	183	2-5	36.1	13.1	50.9
SS2	Lajia site	234	1-2	37.6	11.5	50.9
SS3	Lajia site	121	2-5	37.2	18.2	44.6
SS4	P10 in Fig.1A	99	10-50	70.7	22.2	7.1
SS5	P11 in Fig.1A	343	2-10	56.8	21.9	20.7

Table S3.

Peak discharge of the outburst flood estimated at the dam breach using different formulas, and the outburst volumes of lower and upper condition in Table S1.

Method	Lower condition	Upper condition
	$V=1.13\times10^{10}$ m^3 d=110 m	$V=1.60\times10^{10}$ m^3 d=135 m
$Q=24\ d^{1.73}$ (*36*)	0.08×10^6 m^{3}s^{-1}	0.12×10^6 m^{3}s^{-1}
$Q=3.4\ V^{0.46}$ (*36*)	0.14×10^6 m^{3}s^{-1}	0.17×10^6 m^{3}s^{-1}
$Q=0.3\ (Vd)^{0.49}$ (*36*)	0.25×10^6 m^{3}s^{-1}	0.33×10^6 m^{3}s^{-1}
$Q_{cm}=296\ (HV)^{0.51}$ (*37*)	0.38×10^6 m^{3}s^{-1}	0.51×10^6 m^{3}s^{-1}
$Q=0.063\ (PE)^{0.42}$ (*38*)	0.36×10^6 m^{3}s^{-1}	0.45×10^6 m^{3}s^{-1}
$Q=(8/27)\ Bg^{0.5}d^{1.5}$ (*39*)	0.26×10^6 m^{3}s^{-1}	0.46×10^6 m^{3}s^{-1}

Table S4.

Results of the estimation of the peak discharge of the outburst flood based on Manning's equation (*40*) and the reconstructed cross section 25 km downstream the dam (Fig. S6).

Parameters of the cross section	A=47106 m^2, L=2615 m, R=18.01 m, S=0.002				
Manning coefficient	n=0.05	n=0.04	n=0.035	n=0.03	n=0.02
Average velocity (ms^{-1})	6.2	7.7	8.8	10.2	15.4
Peak discharge (m^3s^{-1})	0.29×10^6	0.36×10^6	0.41×10^6	0.48×10^6	0.72×10^6

Table S5.

Radiocarbon determinations of samples related to the prehistoric outburst flood on the Yellow River. See Fig. S1 for sampling profiles and locations.

Sample no	Sample no (former)	Lab no	Material	^{14}C age 1σ (yr BP)	Calibration with INTCal13 (*31*) and OxCal 4.2 (*32*)	
					result 68% C.I. (BC)	result 95% C.I. (BC)
(A) 1 charcoal sample in silty layer underlying OFS						
P12-1	p-156	BA090139	charcoal	5150±35	4036-4022 (6.2%) 3994-3942 (57.9%) 3854-3846 (2.8%) 3828-3825 (1.3%)	4041-3932 (76.0%) 3874-3808 (19.4%)
(B) 3 bone samples in collapsed cave dwelling F4 at Lajia site						
F4-Ⅹ	F4-Ⅹ	BA110817	bone	3575±40	2010-2000 (4.3%) 1977-1884 (63.9%)	2032-1869 (83.5%) 1846-1776 (11.9%)
F4-Ⅶ	F4-Ⅶ	BA110818	bone	3580±25	1956-1891 (68.2%)	2022-1991 (8.9%) 1984-1882 (86.5%)
F4-Ⅺ	F4-Ⅺ	BA110819	bone	3555±40	1954-1876 (52.8%) 1842-1820 (9.1%) 1796-1781 (6.3%)	2020-1992 (5.1%) 1982-1768 (90.3%)
(C) 17 charcoal samples in OFS						
L-01	XGPS-020-3.9	BA081899	charcoal	4165±35	2874-2850 (11.8%) 2812-2740 (35.4%) 2730-2694 (18.3%) 2686-2680 (2.7%)	2882-2831 (19.6%) 2821-2631 (75.8%)
L-02	XGPS-020-4.0	BA081900	charcoal	3855±35	2452-2420 (11.9%) 2405-2378 (11.8%) 2350-2281 (36.1%) 2249-2232 (7.0%) 2218-2214 (1.4%)	2461-2269 (78.4%) 2260-2206 (17.0%)
L-03	XGPS-020-4.2	BA081901	charcoal	3795±35	2286-2198 (59.1%) 2166-2150 (9.1%)	2397-2385 (0.7%) 2346-2133 (93.4%) 2080-2061 (1.3%)
L-04	XGPS-020-4.6	BA081902	charcoal	4000±35	2566-2521 (46.8%) 2498-2476 (21.4%)	2619-2606 (1.5%) 2599-2593 (0.6%) 2586-2462 (93.3%)
L-05	XGPS-029-6.0	BA081903	charcoal	3855±35	2452-2420 (11.9%) 2405-2378 (11.8%) 2350-2281 (36.1%) 2249-2232 (7.0%) 2218-2214 (1.4%)	2461-2269 (78.4%) 2260-2206 (17.0%)
L-06	XGPS-029-8.8	BA081904	charcoal	3885±35	2457-2339 (66.9%) 2313-2310 (1.3%)	2470-2281 (92.4%) 2250-2232 (2.5%) 2218-2214 (0.5%)
L-07	p-50	BA090129	charcoal	3745±35	2203-2131 (50.7%) 2085-2051 (17.5%)	2280-2249 (7.2%) 2230-2218 (2.0%) 2214-2034 (86.2%)
L-08	p-70	BA090130	charcoal	3705±35	2140-2036 (68.2%)	2201-2016 (92.9%) 1996-1980 (2.5%)
L-09	p-76	BA090131	charcoal	3770±35	2278-2251 (14.6%) 2229-2221 (3.6%) 2210-2138 (49.9%)	2295-2121 (85.7%) 2094-2042 (9.7%)

L-10	p-77	BA090132	charcoal	3895±35	2461-2345 (68.2%)	2474-2286 (95.1%) 2246-2244 (0.3%)
L-11	p-81	BA090133	charcoal	3625±35	2031-1940 (68.2%)	2129-2088 (9.4%) 2047-1892 (86.0%)
L-12	p-93-2	BA090134	charcoal	3730±35	2198-2162 (22.7%) 2152-2126 (16.3%) 2090-2044 (29.2%)	2276-2254 (2.9%) 2210-2028 (92.5%)
L-13	p-93-7	BA090135	charcoal	4050±35	2626-2559 (39.9%) 2536-2491 (28.3%)	2839-2814 (5.9%) 2676-2473 (89.5%)
L-14	LJC-02	BA090384	charcoal	3735±35	2200-2128 (43.8%) 2088-2046 (24.4%)	2277-2252 (4.0%) 2228-2223 (0.6%) 2210-2030 (90.8%)
L-15	p-SLJ-1	BA090140	charcoal	6325±35	5352-5292 (48.9%) 5262-5230 (19.3%)	5371-5218 (95.4%)
P13-1	p-125	BA090136	charcoal	3755±35	2271-2259 (5.1%) 2206-2133 (54.1%) 2081-2060 (8.9%)	2286-2116 (76.7%) 2098-2038 (18.7%)
P9-1	JSX-ED	BA10927	charcoal	3845±35	2429-2425 (1.4%) 2401-2382 (7.5%) 2348-2274 (38.2%) 2256-2208 (21.1%)	2458-2204 (95.4%)
(D) 1 charcoal sample in silty layer overlying OFS						
L-16	Sljc-1	BA090389	charcoal	3550±35	1947-1876 (52.1%) 1841-1821 (9.6%) 1796-1782 (6.6%)	2010-2000 (1.6%) 1977-1770 (93.8%)
(E) 6 charcoal samples in DLS						
P4-1	GPS-035-A	BA081893	charcoal	4065±40	2834-2818 (6.8%) 2662-2646 (5.7%) 2637-2564 (40.2%) 2532-2496 (15.5%)	2856-2811 (12.0%) 2748-2724 (3.3%) 2698-2480 (80.1%)
P4-2	GPS-035-B	BA081894	charcoal	3955±40	2566-2524 (21.8%) 2496-2452 (31.0%) 2419-2406 (5.4%) 2376-2350 (10.0%)	2574-2338 (94.9%) 2314-2310 (0.5%)
P4-3	GPS-038-A	BA081895	charcoal	3550±35	1947-1876 (52.1%) 1841-1821 (9.6%) 1796-1782 (6.6%)	2010-2000 (1.6%) 1977-1770 (93.8%)
P4-4	GPS-038-B	BA081896	charcoal	3610±35	2022-1926 (68.2%)	2120-2096 (3.5%) 2040-1885 (91.9%)
P4-5	GPS-040	BA081897	charcoal	3560±35	1959-1878 (61.5%) 1839-1828 (4.4%) 1792-1785 (2.3%)	2020-1992 (5.3%) 1983-1864 (70.3%) 1850-1773 (19.8%)
P5-1	GPS-033	BA081892	charcoal	3325±40	1658-1599 (36.8%) 1586-1534 (31.4%)	1730-1721 (1.2%) 1692-1506 (94.2%)
(F) 1 sample of plant buried under PLS landslide						
P7-2	JSX-tree	BA07859	branch	2400±40	536-527 (3.7%) 521-404 (64.5%)	748-684 (13.4%) 667-640 (4.3%) 588-578 (0.7%) 562-394 (77.0%)

References

1. X. P. Yuan, W. M. Yan, C. X. Zhang, Y. L. Lou, Eds., *The History of Chinese Civilization*, vol. 1 (Cambridge Univ. Press, New York, 2012).

2. K. C. Chang, *The Archaeology of Ancient China, 4th ed.* (Yale Univ. Press, New Haven and London, 1986).

3. H. Zou, The approach for exploring the culture of Xia. *Henan Wenbo Tongxun* **1**, 34–35 (1978).

4. R. L. Thorp, Erlitou and the search for the Xia. *Early China* **16**, 1–33 (1991).

5. The Xia-Shang-Zhou Chronology Project Group, *The Xia-Shang-Zhou Chronology Project Report for the years 1996–2000 (abridged)* (World Book Publishing Company, Beijing, 2000).

6. L. Liu, X. C. Chen, *The Archaeology of China: From the Late Paleolithic to the Early Bronze Age* (Cambridge Univ. Press, New York, 2012).

7. A. Lawler, Archaeology in China. Founding dynasty or myth? *Science* **325**, 934 (2009). Medline doi:10.1126/science.325_934

8. L. Liu, H. Xu, Rethinking Erlitou: Legend, history and Chinese archaeology. *Antiquity* **81**, 886–901 (2007). doi:10.1017/S0003598X00095983

9. Y. K. Lee, Building the chronology of early Chinese history. *Asian Perspect.* **41**, 15–42 (2002). doi:10.1353/asi.2002.0006

10. S. Allan, The myth of the Xia dynasty. *J. R. Asiat. Soc. GB. Irel.* **116**, 242–256 (1984) (New Series). doi:10.1017/S0035869X00163580

11. M. E. Lewis, *The Flood Myths of Early China* (State Univ. of New York Press, New York, 2006).

12. D. K. Pang, Extraordinary floods in early Chinese history and their absolute dates. *J. Hydro.* **96**, 139–155 (1987). doi:10.1016/0022-1694(87)90149-1

13. X. Q. Li, Lun Bin Gong xu jiqi zhongyao yiyi (On the significance of the Duke Bin Xu vessel). *Zhongguo Lishi Wenwu* **2002**, 4–12 (2002) (Journal of National Museum of Chinese History).

14. W. X. Wu, Q. S. Ge, The possibility of occurring of the extraordinary floods on the eve of the establishment of the Xia dynasty and the historical truth of the Dayu's successful regulating of floodwaters. *Quaternary Science* **25**, 741–749 (2005).

15. C. Lyell, *Principles of Geology*, 9th ed. (Little, Brown & Co., 1853).

16. Methods are available as supplementary materials on *Science* Online.

17. Q. L. Wu, P. Z. Zhang, H. P. Zhang, M. L. Ye, Z. Q. Zhang, A palaeo-earthquake induced damming and bursting of the Yellow River and the abnormal flood that destroyed Lajia Relic. *Sci. China Ser. Dokl. Earth Sci.* **39**, 1148–1159 (2009).

18. IA CASS, QPICRA (The Institute of Archaeology, Chinese Academy of Sciences, Qinghai Provincial Institute of Antiquity and Archaeology), The Lajia site in Minhe County, Qinghai in 2000. *Chinese Archaeology* **3**, 1–6 (2003).

19. X. Y. Yang, Z. K. Xia, M. L. Ye, Prehistoric disasters at Lajia site, Qinghai, China. *Chin. Sci. Bull.* **48**, 1877–1881 (2003). doi:10.1007/BF03184071

20. H. Lu, X. Yang, M. Ye, K. B. Liu, Z. Xia, X. Ren, L. Cai, N. Wu, T. S. Liu, Culinary archaeology: Millet noodles in Late Neolithic China. *Nature* **437**, 967–968 (2005). 67a Medline doi:10.1038/437967a

21. X. L. Zhang, M. L. Ye, S. H. Qiu, J. Zhong, Radiocarbon dating of Lajia site in Minhe County and preliminary analysis. *Kaogu* **11**, 91–104 (2014).

22. J. E. O'Connor, J. E. Costa, The world's largest floods, past and present: Their causes and magnitudes. U.S. Geological Survey Circular 1254 (U.S. Department of the Interior, 2004); http://pubs.usgs.gov/circ/2004/circ1254/pdf/circ1254.pdf.

23. S. G. Evans, K. B. Delaney, R. L. Hermanns, A. Strom, G. Scarascia-Mugnozza, The formation and behaviour of natural and artificial rockslide dams: Implications for engineering performance and hazard management, in *Natural and Artificial Rockslide Dams*, S. G. Evans, K. B. Delaney, R. L. Hermanns, A. Strom, G. Scarascia-Mugnozza, Eds. (Springer, 2011), pp. 1–75.

24. Q. Wang, Discussion on the prehistoric channel shifting of the lower Yellow River and development of regional cultures. *Cultural Relics of Central China* **1993**, 63–72 (1993).

25. D. N. Keightley, The environment of ancient China, in *The Cambridge History of Ancient China*. M. Loewe, E. L. Shaughnessy, Eds. (Cambridge Univ. Press, New York, 1999), pp. 30–36.

26. Y. Wang, H. Cheng, R. L. Edwards, Y. He, X. Kong, Z. An, J. Wu, M. J. Kelly, C. A. Dykoski, X. Li, The Holocene Asian monsoon: Links to solar changes and North Atlantic climate. *Science* **308**, 854–857 (2005). Medline doi:10.1126/science.1106296

27. A. M. Rosen, J. Lee, M. Li, J. Wright, H. T. Wright, H. Fang, The Anthropocene and the landscape of Confucius: A historical ecology of landscape changes in northern and eastern China during the middle to late-Holocene. *Holocene* **25**, 1640–1650 (2015). doi:10.1177/0959683615594241

28. D. S. Nivison, K. D. Pang, Astronomical evidence for the Bamboo Annuals' Chronicle of early Xia. *Early China* **15**, 87–95 (1990).

29. J. Y. Han, *The Environment and Cultural Development in Pre-Qin Northwestern China* (Wenwu Press, Beijing, 2008). pp. 40–468.

30. M. H. Wang, The skeletons and related problems in Lajia site in Minhe County, Qinghai Province. *Kaogu* **2002**, 1081–1084 (2002).

31. P. J. Reimer, E. Bard, A. Bayliss, J. W. Beck, P. G. Blackwell, C. B. Ramsey, C. E. Buck, H. Cheng, R. L. Edwards, M. Friedrich, P. M. Grootes, T. P. Guilderson, H. Haflidason, I. Hajdas, C. Hatté, T. J. Heaton, D. L. Hoffmann, A. G. Hogg, K. A. Hughen, K. F. Kaiser, B. Kromer, S. W. Manning, M. Niu, R. W. Reimer, D. A. Richards, E. M. Scott, J. R. Southon, R. A. Staff, C. S. M. Turney, J. van der Plicht, IntCal13 and Marine13 radiocarbon age calibration curves 0–50,000 years cal BP. *Radiocarbon* **55**, 1869–1887 (2013). doi:10.2458/azu_js_rc.55.16947

32. University of Oxford, OxCal/ORAU; https://c14.arch.ox.ac.uk/oxcal/OxCal.html.

33. A. Jarvis, H. I. Reuter, A. Nelson, E. Guevara, 2008, Hole-filled SRTM for the globe Version 4, available from the CGIAR-CSI SRTM 90m Database (http://www.cgiar-csi.org/data/srtm-90m-digital-elevation-database-v4-1).

34. T. L. Wahl, Uncertainty of predictions of embankment dam breach parameters. *J. Hydraul. Eng.* **130**, 389–397 (2004). doi:10.1061/(ASCE)0733-9429(2004)130:5(389)

35. C. Thornton, M. Pierce, S. Abt, Enhanced predictions for peak outflow from breached embankment dams. *J. Hydrol. Eng.* **16**, 81–88 (2011). doi:10.1061/(ASCE)HE.1943-5584.0000288

36. D. A. Cenderelli, Floods from natural and artificial dam failures, in *Inland Flood Hazards: Human, Riparian and Aquatic Communities*, E. Wohl, Ed. (Cambridge Univ. Press, New York, 2000), pp. 73–103.

37. V. R. Baker, G. Benito, A. N. Rudoy, Paleohydrology of late pleistocene superflooding, Altay Mountains, Siberia. *Science* **259**, 348–350 (1993). Medline doi:10.1126/science.259.5093.348

38. J. E. Costa, R. L. Schuster, The formation and failure of natural dams. *Geol. Soc. Am. Bull.* **100**, 1054–1068 (1988). doi:10.1130/0016-7606(1988)100<1054:TFAFON>2.3.CO;2

39. H. Chanson, Ed., *Hydraulics of Open Channel Flow: An Introduction (2nd ed.)* (McGraw Hill, Oxford, 2004).

40. R. Manning, On the flow of water in open channels and pipes. *Tran. Inst. Civ. Eng. Ir.* **20**, 161–207 (1891).

41. F. C. Shi, Y. J. Yi, P. Mu, Ed., *Investigation and Research of Historical Floods of the Yellow River* (Yellow River Conservancy Press, Zhengzhou, 2002).

42. H. L. de Vries, G. W. Barendsen, Measurements of age by the carbon-14 technique. *Nature* **174**, 1138–1141 (1954). doi:10.1038/1741138a0

43. T. Brown, D. Nelson, J. Vogel, Improved collagen extraction by modified Longin method. *Radiocarbon* **30**, 171–177 (1988).

44. R. E. M. Hedges, G. J. van Klinken, A review of approaches in the pretreatment of bone for radiocarbon dating by AMS. *Radiocarbon* **34**, 279–291 (1992).

45. M. J. Nadeau, M. Schleicher, P. M. Grootes, H. Erlenkeuser, A. Gottdang, D. J. W. Mous, J. M. Sarnthein, H. Willkomm, The Leibniz-Labor AMS facility at the Christian-Albrechts University, Kiel, Germany. *Methods Phys. Res. Sect. B Beam Interact. Mater. Atoms* **123**, 22–30 (1997). doi:10.1016/S0168-583X(96)00730-6

46. G. M. Santos, J. R. Southon, K. C. Druffel-Rodriguez, S. Griffin, M. Mazon, Magnesium perchlorate as an alternative water trap in AMS graphite sample preparation: A report on sample preparation at the KCCAMS Facility at the University of California, Irvine. *Radiocarbon* **46**, 165–173 (2004).

47. X. D. Chen, Ed., *The Hydrology of the Yellow River* (Yellow River Conservancy Press, Zhengzhou, 1996).